

Controlled Transport Based on Multiorbital Aharonov-Bohm Photonic Caging

Gabriel Cáceres-Aravena, Diego Guzmán-Silva[✉], Ignacio Salinas[✉], and Rodrigo A. Vicencio[✉]

Departamento de Física, Facultad de Ciencias Físicas y Matemáticas, Universidad de Chile, Chile and Millennium Institute for Research in Optics—MIRO, Universidad de Chile, Chile

 (Received 27 January 2022; accepted 3 June 2022; published 23 June 2022)

The induction of synthetic magnetic fields on lattice structures allows an effective control of their localization and transport properties. In this Letter, we generate effective π magnetic fluxes on a multiorbital diamond lattice, where first-order (S) and second-order (P) modes effectively interact. We implement a z -scan method on femtosecond-laser-written photonic lattices and experimentally observe Aharonov-Bohm caging for S and P modes, as a consequence of a band transformation and the emergence of a spectrum composed of three degenerated flat bands. As an application, we demonstrate a perfect control of the dynamics, where we translate an input excitation across the lattice in a completely linear and controlled way. Our model, based on a flat band spectrum, allows us to choose the direction of transport depending on the excitation site or input phase.

DOI: [10.1103/PhysRevLett.128.256602](https://doi.org/10.1103/PhysRevLett.128.256602)

Understanding the properties of transport and localization in lattice systems has been crucial for the implementation of present technologies based in electronics. Novel phenomena have been discovered where, for example, the transport can be drastically reduced and localization effects could emerge. One important example is the well-known Anderson localization [1], where all the eigenmodes collapse due to a destructive interference process associated with a random distribution of the site energies and/or lattice positions [2,3]. Another interesting and more controllable method appears with the addition of a magnetic flux on a lattice, which adds an extra phase on hopping (coupling) coefficients. For very specific values of this flux, a phenomenon of extreme localization is observed, the so-called *Aharonov-Bohm (AB) caging* [4–6]. In this case, in contrast to the Anderson localization, all the eigenmodes become degenerate and form a set of flat bands (FBs) [7]. Therefore, an input excitation is decomposed in FB compact states, the energy is caged, and the transport is abruptly reduced into a couple of unit cells. Although the use of a magnetic flux was initially thought of for electronic lattices, it is possible to map its effect to nonelectronic systems by the use of artificial gauge fields [8]. This opens the possibility to study the AB effect in other physical systems [9–15], as well as to experimentally observe it in superconducting wire networks [16] and in semiconductors tailored in an electron gas [17]. Very recently, a synthetic magnetic flux has been implemented in photonics by applying a detuning and modulation of curved waveguides [18], by the addition of auxiliary waveguides to generate an effective negative coupling [19], or by the excitation of special beams having orbital angular momentum [20].

While the AB effect allows us to trap and steer the propagation of light on a given region, other ways of

controlling the dynamics in optical lattices have been suggested as well [21]. When studying mobility properties to, for example, modify the direction of propagation of a light beam, most of the efforts have been focused on the addition of nonlinearity to the system [21–25], which also induces instabilities and resonances with linear modes. Interestingly, magnetic fluxes in non-Hermitian lattices also have the property to alter the direction of propagation, affecting both reflection and transmission, and producing unidirectional reflection, absorption, and lasing [26–31]. However, the control of localized wave packets, including a magnetic flux in Hermitian systems, has not been experimentally observed so far. A controlled flow of energy is important in general physics and also when thinking on concrete applications, such as, for example, logical operations and concatenated optical gates in photonics and integrated circuits [32,33].

In this Letter, we propose a novel form to implement a synthetic magnetic flux in lattices via the use of interorbital coupling [34] on a diamond lattice [9]. By considering the effective interaction between fundamental (S) and second-order (P) modes, a positive and negative coupling can be obtained depending on waveguide and mode orientation. This allows us to induce an effective magnetic flux $\phi = \pi$ per plaquette (a closed ring in the lattice), allowing a direct observation of AB caging. By using a femtosecond (fs) laser writing technique [35], we fabricate a multiorbital photonic lattice having a mixture of straight waveguides which support one or two modes. We observe quite clearly AB caging for S and P states. As a remarkable application, we experimentally demonstrate a novel mechanism for directional transport of linear localized excitations. We show a perfect steering of the energy across the lattice in a very compact way and suggest a concatenated photonic

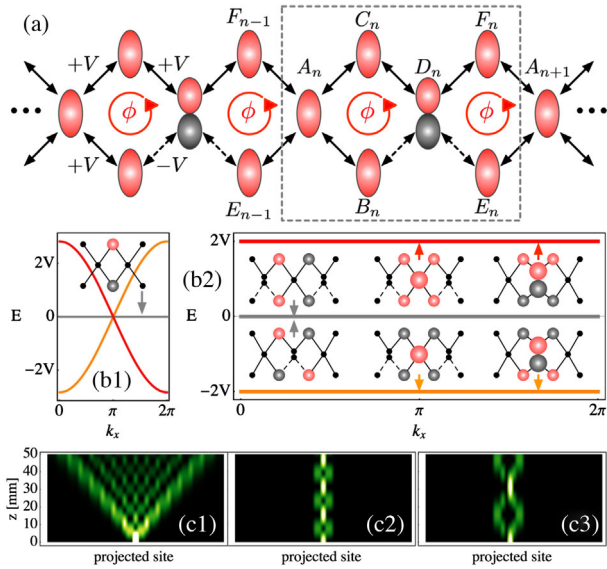


FIG. 1. (a) A multi-orbital diamond lattice formed by S and P sites. Full (dashed) arrows indicate a positive (negative) coupling constant. The effective induced magnetic flux per plaquette is denoted as ϕ . A dashed rectangle defines the unit cell formed by six lattice sites. (b1),(b2) Spectra for $\phi = 0$ and $\phi = \pi$, respectively. FB profiles are shown as insets. (c) Intensity evolution for different input conditions: (c1) central site for $\phi = 0$; (c2) central site for $\phi = \pi$; (c3) top or bottom site for $\phi = \pi$. In (c1)–(c3), $V = 0.1 \text{ mm}^{-1}$ and $z_{\text{max}} = 50 \text{ mm}$.

scheme. Our results are certainly a step forward on the study of discrete dynamics [36,37], offering a new and linear solution for the mobility of localized wave packets in lattices.

Our model consists of a multi-orbital diamondlike chain, which includes sites that support fundamental modes only and sites that also support a second mode, as is sketched in Fig. 1(a). As the mathematical model is equivalent to the propagation of quantum particles on a tight-binding lattice, we use the hydrogen-like nomenclature of S and P orbitals. We have very recently demonstrated [34] that an effective interaction between different orbitals can be achieved when a tuning process is implemented, such that the optical propagation constants (or the energies in a quantum version) match. This also means that the S mode of tuned P sites is no longer in resonance with the S mode of S sites, and therefore they simply do not interact. The unit cell of this lattice consists of six sites as shown by a dashed rectangle in Fig. 1(a). The coupling interaction between sites is determined by the coupling constants $\pm V$, which depend on the spatial orientation of waveguides and their respective modes. We have defined the positive part of the wave functions using red colors, while the negative part is in gray. For any distance, the horizontal coupling in between S and P waveguides, at the central row, is zero due to the orthogonality of both wave functions and the π phase structure of the P mode [38]. In fact, this makes it

possible to achieve positive and negative coupling constants on a given lattice geometry and to induce new phenomena on rather trivial systems, without the need of implementing more complex configurations [18–20].

A single negative coupling constant on a plaquette effectively induces a synthetic flux of $\phi = \pm\pi$ [9], which is the main requirement for the observation of AB caging. We use a tight-binding approach to write down the coupled equations governing the dynamics of this system [39], which in a compact form can be written as

$$-i \frac{\partial \psi_n}{\partial z} = \sum_m V_{n,m} \psi_m. \quad (1)$$

Here, $\psi_n(z)$ describes all the lattice amplitudes, z the propagation distance (dynamical coordinate), and $V_{n,m}$ the nearest-neighbor coupling elements. First of all, we look for the lattice spectrum by assuming a Bloch ansatz of the form $\psi_n(z) = \psi_0 \exp\{ik_x n\}$, with ψ_0 being a site amplitude and k_x the horizontal quasimomentum. We notice that for a homogeneous lattice, composed of S waveguides only, the effective flux is simply $\phi = 0$, the unit cell reduces to only three sites, and the spectrum has just three bands [9]: $E = 0, \pm 2\sqrt{2} \cos(k_x/2)$. We plot this spectrum in Fig. 1(b1) and observe a FB with compact localized states [7,43], such as the ones shown in the inset. FB localization is typically achieved by destructive interference of positive and negative amplitudes at specific connector sites [7,44], which, in this case, correspond to the ones in the central row. Therefore, the excitation of central sites does not resonate with FB states and excites dispersive bands only (more details in Ref. [39]), as the numerical propagation shows in Fig. 1(c1).

On the other hand, a multi-orbital lattice such as the one shown in Fig. 1(a) induces an effective flux of π at closed plaquettes. This small modification on coupling coefficients produces a fundamental change on the linear properties: all the linear modes become compact and completely localized. The synthetic magnetic field cancels the lattice dispersion, and no extended eigenmodes are allowed to exist in the system. The linear spectrum has six bands with only three different eigenvalues (each band having a twofold degeneracy):

$$E_0 = 0, \quad E_+ = 2V, \quad E_- = -2V.$$

This flat spectrum is shown in Fig. 1(b2), including the six different FB states as insets. We immediately notice that a single-site excitation will excite a reduced number of FB states only. The AB caging is usually understood [18–20] as a symmetric oscillation of the energy on a narrow lattice region, as a consequence of exciting a couple of localized FB states corresponding to two different energies. When injecting light at sites S or P at the central row, only two FB states will be excited with energies $\pm 2V$, with a caging

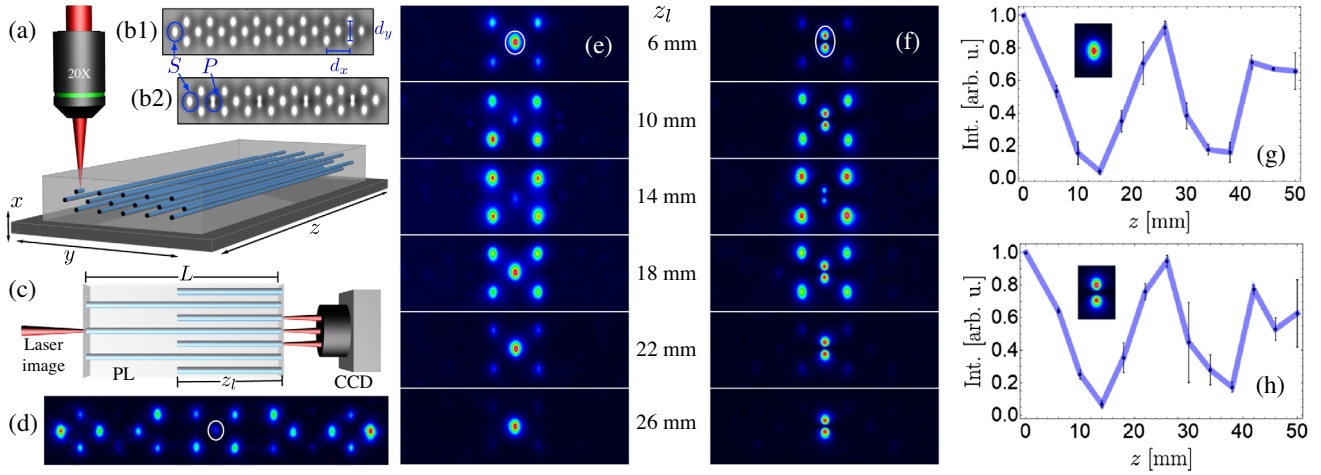


FIG. 2. (a) Femtosecond laser writing technique. (b1),(b2) Bright-field microscopy images for homogeneous and multiorbital diamond lattices, respectively. (c) Top view of the image characterization setup and z -scan concept. (d) Intensity output image at $z = L$ for $\phi = 0$. (e),(f) Intensity output images at $z = z_l$ and $\phi = \pi$, for an S -mode and a P -mode excitation, respectively. A circle shows the input site in (d)–(f). (g),(h) Average intensity at the input waveguide versus propagation length z_l , for an S -mode and a P -mode excitation, respectively. Error bars correspond to the standard deviation.

period of $z_c = \pi/2V$ [39]. We simulate this scenario in Fig. 1(c2), where a central-row site (S or P) is excited. We observe how the energy is trapped and goes back and forward, oscillating around the input position—i.e., the energy is caged. A perfect destructive interference occurs at the next central sites, and no amplitude is transmitted to the rest of the lattice. As a consequence, the energy returns back to the input position, and a caging cycle starts again. Figure 1(c3) likewise shows a periodic dynamics when light is injected at the top or bottom S sites, as a result of exciting three FBs [39].

We fabricate a set of photonic lattices (PLs) by using a femtosecond laser writing technique [35], which is sketched in Fig. 2(a). In this technique, pulses of ~ 240 fs and ~ 82 mW are tightly focused inside a borosilicate glass wafer of length $L = 50$ mm, while a high-precision XYZ Aerotech stage translates the wafer at a velocity of 0.4 mm/s. We start by fabricating a homogeneous diamond S lattice as shown in Fig. 2(b1), with nominal distances $\{d_x, d_y\} = \{36.00, 29.72\}$ μm . We experimentally test the lattices by using an image setup [39,45], which modulates in amplitude and phase a wide laser beam of 640 nm. We image a specific input condition onto the PL input facet, as sketched in Fig. 2(c), and we measure the output profile using a CCD camera. For the homogeneous lattice, we excite a single S waveguide and observe a well-diffracted spatial profile, as shown in Fig. 2(d). We notice that the energy covers all the lattice, as a result of exciting only the dispersive part of the spectrum [39]. We increase the writing power to 104 mW for the P waveguides (four in our experiment), which are located in the central row, as shown in Fig. 2(b2). The writing powers were chosen to reach a maximum coupling in between the S and P modes [34], which occurs when

their propagation constants are precisely tuned [39]. We implement a z -scan method to characterize the dynamics along the propagation coordinate and fabricate twelve multiorbital lattices. All S and P waveguides at the central row have a full length L , while the rest of the waveguides in the top and bottom rows have a shorter propagation length z_l , from 6 to 50 mm in steps of 4 mm, as sketched in Fig. 2(c). In this way, by exciting a single S or P waveguide at the central row, we are able to trace the dynamics at different distances.

First of all, we excite an S central site and observe quite clearly S -mode caging in Fig. 2(e), for the distances indicated in the central column. We observe that the light is able to couple to the top and bottom nearest-neighbour sites, but it cannot propagate further through the lattice due to destructive interference at the next central sites. We measure the output intensity at the input site for different z_l values and plot the data in Fig. 2(g), where we average the data for the three central S waveguides of our lattice. The light oscillates twice for 50 mm, with a caging period of $z_c \approx 26$ mm, which implies a coupling of $V \approx 0.06$ mm^{-1} . The numerical simulation shown in Fig. 1(c2) describes an oscillation for S and P modes. Therefore, we should observe a similar caging phenomena also by using a P mode as an input condition, which consists of two lobes with a π phase difference. The output profiles obtained after exciting the lattice with a second mode at P central waveguides are shown in Fig. 2(f). We nicely and quite clearly observe AB caging for a P mode. The light tries to escape from the input site and couple to its neighbor S waveguides, but it already has a phase difference due to the P parity. This makes it impossible for the light to continue escaping because of the destructive interference occurring at the next central S sites. Therefore, an effective wall is

created due to the induced synthetic magnetic field, and the light is reflected back into the input position, and the cycle starts again. In Fig. 2(h), we observe a two-cycle oscillation in 50 mm and a similar caging period for a second mode excitation (we averaged the data considering the four central P waveguides). In both cases, we observe that more than 90% of the energy is caged in a first cycle, with an intensity reduction after two beating lengths. As perfect tuning and perfect coupling symmetry conditions are really hard to achieve experimentally, we expect to have some dispersion while increasing the propagation distance. Once the destructive interference is not perfectly balanced due to any symmetry-breaking mechanism, some energy will be radiated through the lattice. Nevertheless, we observe in Figs. 2(e)–2(h) that most of the energy is very well confined in a narrow spatial region, and that a multiorbital caging is clearly demonstrated [18–20].

We notice that in a homogenous array, the transport is uniformly distributed in both directions [see Fig. 2(d)], while when using a multiorbital mask, an unidirectional displacement could be observed, allowing us to decide if the light propagates to the right or to the left of the system. We fabricate a smaller multiorbital lattice, which we call an *optical mask*, as the one sketched in Fig. 3(a). Again, we implement a z -scan study by fabricating 12 lattices, where the S top and bottom sites of the central column have a full length L , while the rest of the lattice sites have a shorter propagation distance z_l , which goes from 4 to 26 mm in steps of 2 mm. We expect to observe a maximum translation of the energy at $z_l \sim 26$ mm (in our mask, the effective transversal translation is similar to the one for the AB caging, as we need to move from two S sites into similar S sites to the right or to the left). The experiment consists of exciting simultaneously two full-length S sites at the center of the lattice using an image setup [39]. An in-phase ($++$) excitation [shown in the left panel of Fig. 3(a)] produces a perfect cancellation of amplitudes at the right P central waveguide, and therefore allows zero energy flowing to the right of the mask. In contrast, the light will propagate to the left, as the first coupling occurs with the central S site only, which then couples with the following (left) top and bottom S sites. There, a perfect full translation is achieved with precise control and discrete energy transportation from one unit cell into another. The energy in this case cannot continue moving to the next P waveguide: the energy finds an interference wall and the light is reflected back again to the input position, in a dynamical picture similar to the caging one described previously. The experimental intensity images obtained in this experiment are shown in Fig. 3(b1), where we observe how the light is not allowed to propagate to the right and is only able to move to the left. In fact, our experiment nicely shows how the input condition has been precisely translated to the left in a distance $z_l \approx 24$ mm. Of course, this input condition also excites a caging-like transport due to the presence of

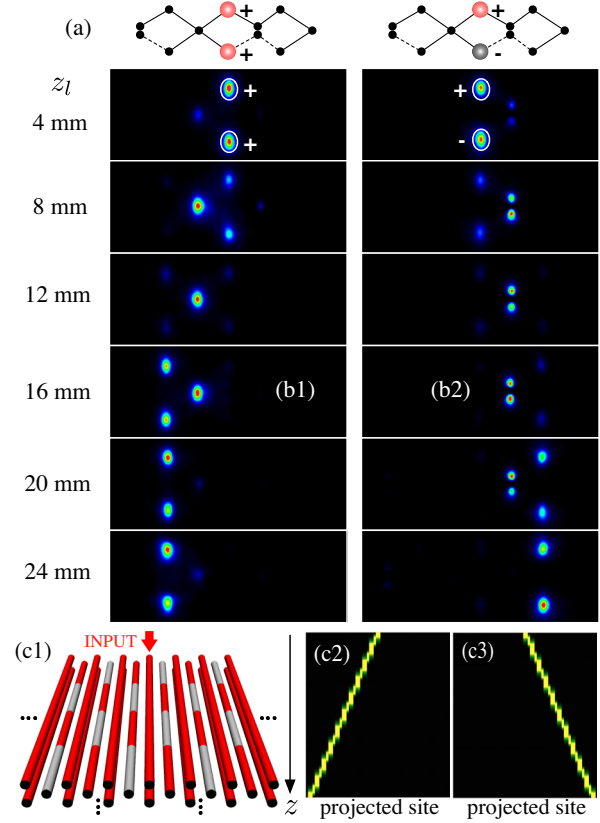


FIG. 3. (a) Optical mask with an in-phase (left) and an out-of-phase (right) input excitation. (b1),(b2) Intensity output images at $z = z_l$ and $\phi = \pi$, for in-phase and out-of-phase input excitations, respectively. Circles show the input sites. (c1) Concatenation scheme: red and gray colors correspond to S and P waveguides, respectively. (c2),(c3) Numerical propagation for in-phase and out-of-phase input conditions, respectively.

only FBs in the spectrum, and the energy oscillates in a very well-defined region. For a longer propagation, the energy will go back and will replicate the in-phase input profile. The out-of-phase ($+ -$) input condition shown in the right panel of Fig. 3(a) will show the opposite dynamics. The destructive interference will cancel the amplitude at the left S central site, and no energy will flow to the left. However, the π phase difference will cancel the effect of the negative coupling, and the energy will flow through the P central site while keeping the initial phase difference. Therefore, when arriving at a S central site to the right, the amplitude will simply be zero there. The experimental images showing the out-of-phase case are presented in Fig. 3(b2).

As a concrete and very important application, we numerically show that by concatenating several optical masks, as is schematically described in Fig. 3(c1) [every mask shifts the S and P central waveguides periodically in the propagation direction], we achieve a controlled displacement on a larger lattice structure. A perfect translation of the energy (to the right or to the left) is obtained, as the numerical simulations in Figs. 3(c2) and 3(c3) indicate.

In fact, by changing the input phase or input position, one can reverse the direction of movement. For example, an in-phase profile could move to the left in position $\{B_n, C_n\}$ and to the right in positions $\{E_{n\pm 1}, F_{n\pm 1}\}$. This is a very remarkable result for lattice systems [36,37], considering that our proposal is based on linear properties only. We therefore suggest a simple and clear method for perfect energy transport, with high controllability and stability. The injection of in-phase or out-of-phase input conditions allows us to propagate the energy freely through the lattice, while on the other hand, the injection of S or P states at the central row induces AB caging. Therefore, our lattice model gives a perfect linear solution for controlled transport and localization.

In conclusion, we have proposed a new scheme for inducing synthetic magnetic fields in lattice systems. This effect relies on the interaction between fundamental S and excited P modes, observing a net flux of π per plaquette [46]. We experimentally proved this system by fabricating multiorbital diamond photonic lattices, and we observed Aharonov-Bohm caging for both modes, which is a direct experimental proof for the induction of an effective magnetic field. We demonstrated the possibility of controlling the direction of transportation determined by the input condition, and therefore, our proposal gives a simple on-demand solution for localization and transport in lattices. We believe that our multiorbital configuration has the flexibility to include more effects in a following study, such as non-Hermiticity [47] or nonlinear effects [48], in a very closed and direct form. Our findings could be particularly useful in the creation and manipulation of concatenated logic gates [32,33], where an external control [49] of the lattice properties could be a promising direction of applied research in quantum computing [50].

The authors acknowledge stimulating discussions with Magnus Johansson and Bastian Real. This work was supported in part by Millennium Science Initiative Program ICN17_012, and FONDECYT Grants No. 1191205 and No. 3190601.

G. C.-A. and D. G.-S. contributed equally to this work.

[1] P. W. Anderson, *Phys. Rev.* **109**, 1492 (1958).
 [2] T. Schwartz, G. Bartal, S. Fishman, and M. Segev, *Nature (London)* **446**, 52 (2007).
 [3] Y. Lahini, A. Avidan, F. Pozzi, M. Sorel, R. Morandotti, D. N. Christodoulides, and Y. Silberberg, *Phys. Rev. Lett.* **100**, 013906 (2008).
 [4] Y. Aharonov and D. Bohm, *Phys. Rev.* **115**, 485 (1959).
 [5] J. Vidal, R. Mosseri, and B. Douçot, *Phys. Rev. Lett.* **81**, 5888 (1998).
 [6] J. Vidal, B. Douçot, R. Mosseri, and P. Butaud, *Phys. Rev. Lett.* **85**, 3906 (2000).
 [7] R. A. Vicencio, *Adv. Phys.* **6**, 1878057 (2021).

[8] M. Aidelsburger, S. Nascimbene, and N. Goldman, *C.R. Phys.* **19**, 394 (2018).
 [9] S. Longhi, *Opt. Lett.* **39**, 5892 (2014).
 [10] K. Fang, Z. Yu, and S. Fan, *Phys. Rev. Lett.* **108**, 153901 (2012).
 [11] I. Bloch, J. Dalibard, and S. Nascimbène, *Nat. Phys.* **8**, 267 (2012).
 [12] V. Brosco, L. Piloizzi, and C. Conti, *Phys. Rev. B* **104**, 024306 (2021).
 [13] H. Perrin, J.-N. Fuchs, and R. Mosseri, *Phys. Rev. B* **101**, 235167 (2020).
 [14] G. Möller and N. R. Cooper, *Phys. Rev. Lett.* **108**, 045306 (2012).
 [15] A. Bermudez, T. Schaetz, and D. Porras, *Phys. Rev. Lett.* **107**, 150501 (2011).
 [16] C. C. Abilio, P. Butaud, T. Fournier, B. Pannetier, J. Vidal, S. Tedesco, and B. Dalzotto, *Phys. Rev. Lett.* **83**, 5102 (1999).
 [17] C. Naud, G. Faini, and D. Maily, *Phys. Rev. Lett.* **86**, 5104 (2001).
 [18] S. Mukherjee, M. Di Liberto, P. Öhberg, R. R. Thomson, and N. Goldman, *Phys. Rev. Lett.* **121**, 075502 (2018).
 [19] M. Kremer, I. Petrides, E. Meyer, M. Heinrich, O. Zilberberg, and A. Szameit, *Nat. Commun.* **11**, 907 (2020).
 [20] C. Jörg, G. Queraltó, M. Kremer, G. Pelegrí, J. Schulz, A. Szameit, G. von Freymann, J. Mompart, and V. Ahufinger, *Light* **9**, 150 (2020).
 [21] I. L. Garanovich, S. Longhi, A. A. Sukhorukov, and Y. S. Kivshar, *Phys. Rep.* **518**, 1 (2012).
 [22] M. I. Molina, I. L. Garanovich, A. A. Sukhorukov, and Y. S. Kivshar, *Opt. Lett.* **31**, 2332 (2006).
 [23] U. Naether, R. A. Vicencio, and M. Stepić, *Opt. Lett.* **36**, 1467 (2011).
 [24] C. Mejía-Cortés, R. A. Vicencio, and B. A. Malomed, *Phys. Rev. E* **88**, 052901 (2013).
 [25] U. Peschel, R. Morandotti, J. M. Arnold, J. S. Aitchison, H. S. Eisenberg, Y. Silberberg, T. Pertsch, and F. Lederer, *J. Opt. Soc. Am. B* **19**, 2637 (2002).
 [26] L. Jin, X. Z. Zhang, G. Zhang, and Z. Song, *Sci. Rep.* **6**, 20976 (2016).
 [27] A. Regensburger, C. Bersch, M.-A. Miri, G. Onishchukov, D. N. Christodoulides, and U. Peschel, *Nature (London)* **488**, 167 (2012).
 [28] L. Feng, Y.-L. Xu, W. S. Fegadolli, M.-H. Lu, J. B. Oliveira, V. R. Almeida, Y.-F. Chen, and A. Scherer, *Nat. Mater.* **12**, 108 (2013).
 [29] H. Ramezani, H.-K. Li, Y. Wang, and X. Zhang, *Phys. Rev. Lett.* **113**, 263905 (2014).
 [30] H. Ramezani, Y. Wang, E. Yablonovitch, and X. Zhang, *IEEE J. Sel. Top. Quantum Electron.* **22**, 115 (2016).
 [31] L. Jin and Z. Song, *Phys. Rev. Lett.* **121**, 073901 (2018).
 [32] D. Pérez, I. Gasulla, P. D. Mahapatra, and J. Capmany, *Adv. Opt. Photonics* **12**, 709 (2020).
 [33] G. Corrielli, A. Crespi, and R. Osellame, *Nanophotonics* **10**, 3789 (2021).
 [34] D. Guzmán-Silva, G. Cáceres-Aravena, and R. A. Vicencio, *Phys. Rev. Lett.* **127**, 066601 (2021).
 [35] A. Szameit, D. Blömer, J. Burghoff, T. Schreiber, T. Pertsch, S. Nolte, A. Tünnermann, and F. Lederer, *Opt. Express* **13**, 10552 (2005).

- [36] F. Lederer, G. I. Stegeman, D. N. Christodoulides, G. Assanto, M. Segev, and Y. Silberberg, *Phys. Rep.* **463**, 1 (2008).
- [37] S. Flach and A. V. Gorbach, *Phys. Rep.* **467**, 1 (2008).
- [38] A. Sutton, *Electronic Structure of Materials* (Clarendon Press, Oxford, 1993).
- [39] See Supplemental Material at <http://link.aps.org/supplemental/10.1103/PhysRevLett.128.256602> for more details, which includes Refs. [40–42].
- [40] U. Naether, A. J. Martínez, D. Guzmán-Silva, M. I. Molina, and R. A. Vicencio, *Phys. Rev. E* **87**, 062914 (2013).
- [41] C. Cantillano, S. Mukherjee, L. Morales-Inostroza, B. Real, G. Cáceres-Aravena, C. Hermann-Avigliano, R. R. Thomson, and R. A. Vicencio, *New J. Phys.* **20**, 033028 (2018).
- [42] C. Cantillano, L. Morales-Inostroza, B. Real, S. Rojas-Rojas, A. Delgado, A. Szameit, and R. A. Vicencio, *Sci. Bull.* **62**, 339 (2017).
- [43] S. Mukherjee and R. R. Thomson, *Opt. Lett.* **40**, 5443 (2015).
- [44] L. Morales-Inostroza and R. A. Vicencio, *Phys. Rev. A* **94**, 043831 (2016).
- [45] R. A. Vicencio, C. Cantillano, L. Morales-Inostroza, B. Real, C. Mejía-Cortés, S. Weimann, A. Szameit, and M. I. Molina, *Phys. Rev. Lett.* **114**, 245503 (2015).
- [46] J. Schulz, J. Noh, W. A. Benalcazar, G. Bahl, and G. Von Freymann, [arXiv:2204.06238](https://arxiv.org/abs/2204.06238).
- [47] S. M. Zhang and L. Jin, *Phys. Rev. Research* **2**, 033127 (2020).
- [48] N. Chang, S. Gundogdu, D. Leykam, D. G. Angelakis, S. Kou, S. Flach, and A. Maluckov, *APL Photonics* **6**, 030801 (2021).
- [49] Y.-J. Chang, Y.-H. Lu, Y. Wang, X.-Y. Xu, W.-H. Zhou, W.-H. Cui, X.-W. Wang, J. Gao, L.-F. Qiao, and X.-M. Jin, *Phys. Rev. Lett.* **126**, 110501 (2021).
- [50] J. M. Arrazola *et al.*, *Nature (London)* **591**, 54 (2021).